

Salt Modulated Structure of Polyelectrolyte-Macroion Complex Fibers

Hoda Boroudjerdi¹, Ali Naji^{1,2}, and Roland R. Netz¹

¹ Department of Physics, Technical University of Munich, Garching 85748, Germany

² Department of Applied Mathematics and Theoretical Physics, Centre for Mathematical Sciences, University of Cambridge, Cambridge CB3 0WA, United Kingdom

Received: date / Revised version: date

Abstract. The structure and stability of strongly charged complex fibers, formed by complexation of a single long semi-flexible polyelectrolyte chain and many oppositely charged spherical macroions, are investigated numerically at the ground-state level using a chain-sphere cell model. The model takes into account chain elasticity as well as electrostatic interactions between charged spheres and chain segments. Using a numerical optimization method based on a periodically repeated unit cell, we obtain fiber configurations that minimize the total energy. The optimal fiber configurations exhibit a variety of helical structures for the arrangement of macroions including zig-zag, solenoidal and beads-on-a-string patterns. These structures are determined by a competition between attraction between spheres and the polyelectrolyte chain (which favors chain wrapping around the spheres), chain bending and electrostatic repulsion between chain segments (which favor unwrapping of the chain), and the interactions between neighboring sphere-chain complexes which can be attractive or repulsive depending on the system parameters such as medium salt concentration, macroion charge and chain length per macroion (linker size). At about physiological salt concentration, dense zig-zag patterns are found to be energetically most stable when parameters appropriate for the DNA-histone system in a chromatin fiber are adopted. In fact, the predicted fiber diameter in this regime is found to be around 30 nanometers, which appears to agree with the thickness observed in *in vitro* experiments on chromatin. We also find a macroion (histone) density of 5-6 per 11 nm which agrees with the zig-zag or cross-linker models of chromatin. Since our study deals primarily with a generic chain-sphere model, these findings suggest that structures similar to those found for chromatin should also be observable for polyelectrolyte-macroion complexes formed in solutions of DNA and synthetic nanocolloids of opposite charge. In the ensemble where the mean linear density of spheres on the chain is fixed, the present model predicts a phase separation at intermediate salt concentrations into a densely packed complex phase and a dilute phase.

PACS. 87.15.-v Biomolecules: structure and physical properties – 87.16.Sr Chromosomes, histones – 82.70.-y Disperse systems; complex fluids

1 Introduction

Recent years have witnessed a growing interest in the structure and phase behavior of large charged polymer-macroion clusters, for instance, a long polyelectrolyte (PE) chain is complexed with many oppositely charged spheres [1, 2, 3, 4, 5, 6, 7, 8, 9, 10, 11, 12, 13, 14, 15]. Perhaps, the most striking example is realized in biology, where a huge fiber is formed by complexation of a long (negatively charged) DNA chain with (positively charged) histone proteins, giving rise to the prominent *chromatin fiber* [16, 17, 18, 19, 20, 21, 22, 23]. The fundamental unit of chromatin is known as the *nucleosome* consisting of about 200 base pairs (about 68 nm) of DNA associated with a cylindrical-wedge-shaped histone octamer of diameter about 7 nm and mean height 5.5 nm. The nucleosome has two main parts: i) the *nucleosome core particle* (or the *core particle*) comprising 146

base pairs of DNA wrapped in nearly a 1-and-3/4 left-handed helical turn around the histone octamer, and ii) the *linker DNA*, which connects adjacent core particles to one another. There is an additional component known as linker histone H1 (or its variant H5), which binds to the DNA and the histone octamer in such a way that it brings the entering and exiting strands of DNA together along a short distance, forming a stem-like structure. The role of linker histone will be discussed further below.

In vitro experiments have revealed striking salt-induced conformational changes for the chromatin fiber (see, e.g., [16, 24, 25, 26, 27, 28, 29]): At very small salt concentration, the fiber structure is swollen, displaying an open *beads-on-a-string* pattern in which individual core particles become highly separated from each other; the resultant fiber is known as the *10 nm fiber* because of the nearly 10 nm

hard-core diameter of the core particle (nearly equal to the combined diameter of the core histone octamer and twice that of the DNA wrapped around it). As the salt concentration increases, the fiber becomes more and more folded and finally within the physiologically relevant regime (around 100 mM NaCl), it exhibits a thick and dense fiber of diameter about 30 nm, known as the *30 nm fiber*. This salt-dependent behavior indicates that predominant electrostatic mechanisms are involved and influence the organization of the chromatin fiber.

The precise arrangement of nucleosome core particles in the 30 nm fiber has been under debate for a long time [17, 18, 24, 27, 28, 29, 30, 31, 32, 33, 34, 35, 36, 37, 38, 39, 40, 41, 42, 43, 44, 45, 46, 47, 48, 49, 50, 51, 52, 53]. A large number of models have been proposed for the structure of the 30 nm fiber which are more or less consistent with the experimental observations. For instance, several studies [27, 28, 29, 30] appear to support a zig-zag or cross-linker pattern, where successive nucleosomes are at opposite sides of the fiber and the linker DNA joining them bridges across the helical core of the fiber. Among other models supported by recent experiments are the solenoidal model [24, 31] (in which successive nucleosomes are juxtaposed as nearest neighbors with the linker DNA bent in between them), the twisted ribbon model [32], as well as the more general class of ribbon models [50, 51] (see Refs. [18, 39, 48, 51] for a more comprehensive reference list and discussion of various chromatin models).

Our goal in this work is to address structural properties of generic chain-sphere complex fibers comprising a long semi-flexible charged PE chain and many oppositely charged spheres. We adopt a simple chain-sphere cell-model approach [54, 55] that allows for a systematic description of the polymer conformation in an infinite fiber. The chain conformation and the fiber structure are determined by a competition between chain elasticity, electrostatic interactions (among chain segments and charged spheres across a salt solution) as well as geometrical constraints. We employ a numerical optimization method to find configurations minimizing the total fiber Hamiltonian with respect to the whole conformation of the complexed chain and the position of macroions. This scheme is known as the *ground-state-dominance approximation* which is valid for strongly-coupled charged complexes (such as DNA-histone complexes) that exhibit large PE adsorption energy and relatively small thermal fluctuations [54, 55]. The organization of the chain on individual macroions and hence throughout the fiber is *not* externally imposed, but rather obtained as a result of the interplay between inter- and intra-fiber interactions. We demonstrate that the resultant optimal fiber structures exhibit a variety of helical structures including, for instance, beads-on-a-string, zig-zag, and solenoidal patterns depending on a few basic system parameters, namely, the salt concentration, the macroion charge valency, and the chain length per macroion (or the linker length). Other parameters such as the chain persistence length and its charge density as well as the sphere diameter will be fixed; here we choose the parameter values appropriate for the DNA-histone sys-

tem throughout this study. We should emphasize, however, that the present model is not meant to address the specific problem of the chromatin fiber (as no attempt is made in order to incorporate explicitly the specific structural details of the actual chromatin fiber such as the linker histone, core histone tails, specific binding effects or the precise shape of the histone octamer [16, 18]), but we rather focus on the more general aspects of complex fiber formation in PE-macroion systems. The results are thus also relevant for mixtures of DNA and oppositely charged nano-colloids or synthetic spheres.

We show that the transition between the predicted helical patterns is dictated by the wrapping-dewrapping behavior of the chain as the system parameters vary. For instance, at low salt concentration, the dominant self-repulsion of chain segments leads to dewrapping of the chain from macroions, generating an expanded fiber. In the physiological regime, zig-zag patterns are found to be energetically most stable, because the chain is wrapped around macroions in about a 1-and-3/4 turn for moderate sphere charge [54], which turns out to be about the same degree of DNA-wrapping in the nucleosome core particles. At elevated salt (beyond 100mM monovalent salt), the highly wrapped state of the chain leads to very compact solenoidal structures for the fiber. The predicted structures will be summarized by presenting a two-angle structural diagram in analogy with the two-angle models in Refs. [17, 27]. An important result follows from our model when the chain (linker) length per macroion is treated as a free parameter. It is found that the binding energy (per macroion) takes a non-convex shape at intermediate salt concentrations (when plotted as a function of the chain length per macroion), with a global minimum at a high sphere density, indicating a gas-liquid-type “phase coexistence” along the fiber: Part of the PE chain forms a dense complex fiber with macroions phase-separating from a dilute phase along the fiber consisting only of uncomplexed chain.

In the aforementioned optimization model, the wrapping structure of the chain around individual macroions is not fixed and can vary so as to minimize the effective Hamiltonian of the fiber (unconstrained optimization). This can be thought of as a simple model mimicking linker-histone-depleted chromatin [24]. The 30 nm fiber obtained within the unconstrained optimization model shows a rather small density (number per projected unit length) of macroions along the fiber, i.e., about one macroion per 11 nm, which is comparable with the nucleosome density at relatively small salt concentration (where the chromatin still has a 30 nm diameter [28]), but not with the density of about 6 histones per 11 nm [18, 24, 26, 27, 28, 29] observed in the physiological salt regime.

As noted above, the linker histone H1 “glues” together the entering and exiting strands of the DNA and also stabilizes (“seals off”) the internal structure of the DNA in the nucleosome core particle. It plays a key role in the compaction of the chromatin into a 30 nm fiber [24]. In order to mimic this kind of effect in a very simple way within the present model, we also employ a variant of the opti-

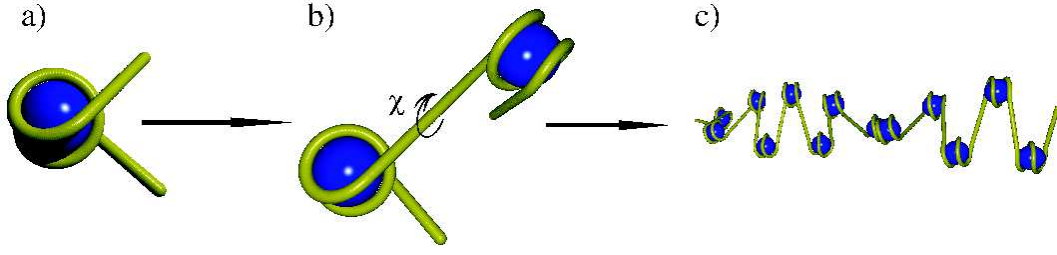


Fig. 1. Cell model for a complex fiber: a) Each unit cell consists of a single PE-macroion complex the precise configuration of which is obtained from a numerical minimization method. b) Two adjacent unit cells (which are identical in configuration) are linked together such that they share a common tangent vector at the unit cells junction (see text). c) By repeating this procedure the whole complex fiber is constructed from a main unit cell. Within the full minimization scheme, all degrees of freedom associated with a single unit cell (that is the chain beads locations as well as the boundary rotational angle χ) are varied in order to find the optimal configuration minimizing the full effective Hamiltonian of the fiber.

mization scheme, the so-called *constrained optimization*, in which the core complex structure is fixed according to the optimal structure of an isolated complex (with a chain length of 146 DNA base pairs); then only the relative orientation angle of adjacent core particle complexes can vary in order to find the optimal fiber structure. This leads to a number of significant changes. Most notably, the entering and exiting strands of the chain tend to form a cross pattern at physiological salt (producing a small entry-exit angle as compared with the unconstrained model), which resembles the stem-like pattern proposed for H1-stabilized nucleosome [24,27,28]. As a result, the resultant optimal fiber is found to have a more compact zig-zag pattern with a histone density of about 5-6 histones per 11 nm in agreement with Refs. [24,26,27,28,29].

The organization of this paper is as follows: In Section 2, we describe the theoretical model and the numerical method used to study infinite charged complex fibers. In Section 3, the salt-induced structural changes of the fiber are studied within the unconstrained optimization model. The constrained optimization model is analyzed in the following Section 4. We then show in Section 5 how the fiber structure is influenced by variation of the linker length and discuss different thermodynamic ensembles and the possibility of phase separation along the chain.

2 Theoretical model: Cell-model approach

The model used here for the study of complex fibers is based upon the chain-sphere model [54,55], which consists of a single semi-flexible PE chain complexed with an oppositely charged sphere (macroion). Here we use this model to describe an infinite complex fiber made from complexation of a *single* long PE chain with many macroions. We restrict the discussion to strongly coupled complexes and thus employ the ground-state-dominance approximation corresponding to strong adsorption of the PE chain on each sphere [54,55,57].

The main idea here is to apply a *cell-model* approach by describing the complex fiber in terms of identical chain-sphere *unit cells* linked together via the same PE strand.

In analogy with the chromatin fiber, one can thus think of each unit cell as consisting of two main parts: i) the *core-particle complex* (macroion sphere complexed with a chain segment), and ii) the *linker chain* connecting adjacent core particles as shown in Fig. 1.

In our numerical analysis, the complex fiber is constructed by replicating one unit cell (referred to as the main unit cell) infinitely many times such that the *connectivity and smoothness* of the linker chain is preserved. We begin the minimization with a given initial condition, typically, the one in which the structure of the core particle complex in each unit cell corresponds to the energetically optimized configuration in an *isolated* chain-sphere complex with the chain length associated with each core particle being taken to be equivalent to 146 DNA base pairs. This procedure for a single isolated complex has been studied thoroughly in our previous works [54,55,56]. We then connect an arbitrary length of linker chain and the interaction Hamiltonian of the *whole* fiber is minimized using a recursive numerical method to find the optimal fiber structure without any further constraints (see below). This follows simply by focusing on a single unit cell. Although this prescribes a model consisting of identical unit cells, the optimized fiber structures are by no means trivial in the way the unit cells or core particles are arranged. They display a rich structural phase diagram of helical patterns. Note that these helical patterns may or may not exhibit periodic structures (i.e., structures with discrete translational symmetry). In fact, the energetically optimal structures are merely quasi-periodic, i.e., they do not show exact (rational) periodicity but a distribution of periodicities with a sharp peak around a mean value of periodicity (see Ref. [56] for details). We also note that electrostatic interactions between all unit cells are fully taken into account, and thus on this level, the only approximation of the present cell model is that structural symmetry breaking between the unit cells is neglected.

2.1 Main unit cell

Each unit cell consists of a piece of PE chain of length L_c (or an equivalent of $N_{bp} = L_c/(0.34 \text{ nm})$ DNA base

pairs each of length 0.34 nm) with linear charge density of $-\tau$ (in units of the elementary charge e) and bare (unscreened) mechanical persistence length of ℓ_p . The PE chain interacts with a uniformly charged sphere of radius R_s and charge valency Z in a salt solution of concentration C_s . Although the present model is quite general, in making explicit calculations, we set the parameters appropriate for the DNA-histone system by choosing $\tau = 5.88 \text{ nm}^{-1}$ (maximum dissociation of two elementary charges per base pair [58]), $\ell_p = 30 \text{ nm}$ [54,59,60] and $R_s = 5 \text{ nm}$, while L_c , Z and C_s are varied. Note that the sphere radius of $R_s = 5 \text{ nm}$ represents the closest approach of DNA of radius 1 nm on a histone octamer of mean radius of about 4 nm. As in previous studies [54,55], we employ a discretization scheme in order to parametrize the chain conformation as required for numerical analysis. The chain is discretized using $N + 1$ discretization points or *beads* of valency $q = \tau L_c / (N + 1)$ located at positions $\{\mathbf{r}_i^0\}$ (with $i = 0, 1, \dots, N$ and the super-index 0 denoting the *main unit cell*). This amounts to N rigid chain subunits within a unit cell each described by a *bond vector* $\mathbf{u}_i^0 = \mathbf{r}_i^0 - \mathbf{r}_{i-1}^0$ of length $|\mathbf{u}_i^0| = \Delta$ and two polar and azimuthal angles θ_i and ϕ_i with respect to a fixed orthogonal reference [54,55] (N has in general no connection with the number of actual monomers). The location of the central macroion \mathbf{R}^0 in the main unit cell is chosen as the origin, i.e., $\mathbf{R}^0 = \mathbf{0}$. We conventionally discretize each natural DNA base pair into two discrete subunits; therefore $N = 2N_{bp}$ and we have $q = 1$ (i.e., one elementary charge per subunit or two per base pair) for large N when DNA linear charge density is adopted.

2.2 Unit cell replication

Let us assume that the structure of the core-particle complex within the main unit cell is given (from a minimization scheme as discussed later). We construct the complex fiber by attaching an *image* of the main unit cell to it such that the linker chain *tangentially* connects the two unit cells with no kinks at the junction (see Fig. 1); i.e., the last chain bond vector, \mathbf{u}_N^0 , in the main unit cell is chosen as the first bond vector, \mathbf{u}_1^1 , of the first immediate image cell (labeled by super-index 1) and so on for all other image cells in a recursive manner.

Formally, this replication procedure is established by a combined translation and rotation transformation. In general, the position of the i -th chain bead and that of the sphere center in the k -th unit cell (labeled by super-index k), i.e., \mathbf{r}_i^k and \mathbf{R}^k respectively, are obtained as

$$\mathbf{r}_i^k = \mathbf{E} \cdot (\mathbf{r}_i^{k-1} - \mathbf{r}_0^{k-1}) + \mathbf{r}_{N-1}^{k-1} \quad (1)$$

$$\mathbf{R}^k = \mathbf{E} \cdot (\mathbf{R}^{k-1} - \mathbf{r}_0^{k-1}) + \mathbf{r}_{N-1}^{k-1}, \quad (2)$$

from the given configurations in the $(k - 1)$ -th unit cell (labeled by super-index $k - 1$). Here \mathbf{E} is the full rotation matrix around the *common point* or junction $\mathbf{r}_{N-1}^{k-1} = \mathbf{r}_0^k$ of the two adjacent unit cells, which rotates the bond vector

\mathbf{u}_1^k (and in fact the whole k -th unit cell as a rigid body) such that \mathbf{u}_1^k falls onto \mathbf{u}_N^{k-1} to fulfill the smoothness of the chain at the junction. We then allow the image unit cell k to rotate around this common bond vector by an arbitrary (azimuthal) angle χ , see Fig. 1 for an illustration. This angle is indeed a rotational degree of freedom for each unit cell as a whole in addition to other intra-cell degrees of freedom (bead and sphere positions) that is varied in order to minimize the fiber Hamiltonian (see Section 2.4 below).

The rotation matrix \mathbf{E} is obtained as

$$\mathbf{E} = \mathbf{B} \mathbf{X} \mathbf{A} \quad (3)$$

with the matrices \mathbf{A} , \mathbf{X} and \mathbf{B} defined as follows

$$\mathbf{A} = \begin{pmatrix} -\sin \phi_1 & \cos \phi_1 & 0 \\ -\cos \phi_1 \cos \theta_1 & -\sin \phi_1 \cos \theta_1 & \sin \theta_1 \\ \sin \theta_1 \cos \phi_1 & \sin \phi_1 \sin \theta_1 & \cos \theta_1 \end{pmatrix}, \quad (4)$$

$$\mathbf{X} = \begin{pmatrix} \cos \chi & -\sin \chi & 0 \\ \sin \chi & \cos \chi & 0 \\ 0 & 0 & 1 \end{pmatrix}, \quad (5)$$

$$\mathbf{B} = \begin{pmatrix} -\sin \phi_N & -\cos \phi_N \cos \theta_N & \sin \theta_N \cos \phi_N \\ \cos \phi_N & -\sin \phi_N \cos \theta_N & \sin \phi_N \sin \theta_N \\ 0 & \sin \theta_N & \cos \theta_N \end{pmatrix}, \quad (6)$$

where θ_1 and ϕ_1 are the polar and azimuthal angles of \mathbf{u}_1^0 and θ_N and ϕ_N are the polar and azimuthal angles of \mathbf{u}_N^0 . Note that the matrix \mathbf{E} is only a function of the angles $\{\chi, \theta_1, \phi_1, \theta_N, \phi_N\}$.

2.3 Intra-fiber interactions

Because the infinite complex fiber is obtained by replicating identical unit cells, one can focus on the effective Hamiltonian of the main unit cell, which can be written as

$$\mathcal{H} = \mathcal{H}_{\text{self}} + \sum_{k=1}^M \mathcal{H}_{\text{int}}^{0k}, \quad (7)$$

where $\mathcal{H}_{\text{self}}$ gives the *self-energy* of the main unit cell, and $\mathcal{H}_{\text{int}}^{0k}$ accounts for the interactions between the main and the k -th unit cells. The following interactions are included in these two terms: 1) electrostatic interactions between all charged beads along the PE chain with one another and with charged spheres within the linear Debye-Hückel theory (which effectively captures salt screening effects) as well as the mutual interactions between the charged spheres themselves, 2) a short-ranged soft-core excluded-volume repulsion between chain beads and spheres only, which prevents the chain from penetrating the spheres, and 3) the mechanical bending elasticity of the PE chain. Note that the electrostatic contribution to the bending rigidity is explicitly included via the electrostatic self-energy term. In the second term in Eq. (7), we have used a cut-off M to account for the interaction between M consecutive unit cells. We typically choose $M = 5$. As explicitly checked, the results are not influenced by increasing M

$$\mathcal{H}_{\text{self}} = \frac{\ell_B}{\Delta} \sum_{i=2}^N \left\{ 1 - \cos(\theta_i - \theta_{i-1}) + \sin \theta_i \sin \theta_{i-1} \left(1 - \cos(\phi_i - \phi_{i-1}) \right) \right\} \quad (8)$$

$$+ q^2 \ell_B \sum_{i=0}^{N-1} \sum_{j=i+1}^N \frac{e^{-\kappa |\mathbf{r}_i^0 - \mathbf{r}_j^0|}}{|\mathbf{r}_i^0 - \mathbf{r}_j^0|} - \frac{Zq\ell_B}{1 + \kappa R_s} \sum_{i=0}^N \left[\frac{e^{-\kappa(|\mathbf{r}_i^0| - R_s)}}{|\mathbf{r}_i^0|} - A e^{-(|\mathbf{r}_i^0| - R_s)/\alpha} \right]$$

$$\mathcal{H}_{\text{int}}^{0k} = q^2 \ell_B \sum_{i=0}^N \sum_{j=2}^N \frac{e^{-\kappa |\mathbf{r}_i^0 - \mathbf{r}_j^k|}}{|\mathbf{r}_i^0 - \mathbf{r}_j^k|} - \frac{Zq\ell_B}{1 + \kappa R_s} \left[\sum_{i=0}^N \left(\frac{e^{-\kappa(|\mathbf{r}_i^0 - \mathbf{R}^k| - R_s)}}{|\mathbf{r}_i^0 - \mathbf{R}^k|} - A e^{-(|\mathbf{r}_i^0 - \mathbf{R}^k| - R_s)/\alpha} \right) \right. \\ \left. + \sum_{i=2}^N \left(\frac{e^{-\kappa(|\mathbf{r}_i^k| - R_s)}}{|\mathbf{r}_i^k|} - A e^{-(|\mathbf{r}_i^k| - R_s)/\alpha} \right) \right] + \frac{Z^2 \ell_B e^{2\kappa R_s}}{(1 + \kappa R_s)^2} \frac{e^{-\kappa |\mathbf{R}^k|}}{|\mathbf{R}^k|}, \quad (9)$$

further due to the highly screened nature of electrostatic interactions at high salt and/or highly expanded size of unit cells at low salt.

The self-energy of the main unit cell is written in discretized form as

See equation (8) above

(in units of $k_B T$), where the first term is the mechanical bending contribution, the second term is the electrostatic repulsion between chain segments, and the third term represents chain-sphere attraction as well as the soft-core repulsion (which is specified by a repulsion range, α , and strength A , which are fixed at typical values of $A = 0.014 \text{ nm}^{-1}$ and $\alpha = 0.02 \text{ nm}$ [56]). Recall that $\kappa = (8\pi\ell_B C_s)^{1/2}$ is the inverse Debye screening length for monovalent salt with $\ell_B = e^2/(4\pi\epsilon_0 k_B T)$ being the Bjerrum length.

The interaction between the main unit cell and the k -th image unit cell reads (in units of $k_B T$)

See equation (9) above

noting that the first two beads $i = 0, 1$ for the k -th image unit cell are counted as the last beads of the $(k-1)$ -th cell as explained before. The first term in Eq. (9) corresponds to repulsion between chain segments in the main unit cell and those in the k -th image cell, the second term involves electrostatic attraction and soft-repulsion between the chain segment in the main unit cell and the sphere in the k -th image cell and vice versa. The last term represents electrostatic repulsion between the spheres in the two unit cells.

2.4 Numerical method: Unconstrained (full) minimization model

For strongly coupled PE-macroion complexes (i.e., with large polymer adsorption energy), the so-called ground-state-dominance approximation becomes accurate [54]. Here, one seeks the *optimal* or *ground-state* configuration of the fiber minimizing the effective Hamiltonian (7) with respect to all degrees of freedom that are necessary to specify the

overall chain conformation. This amounts to $2N + 1$ independent degrees of freedom (per unit cell) $\{\theta_i, \phi_{i \neq P}, r_P, \chi\}$, where θ_i and $\phi_{i \neq P}$ are the chain's bond vector angles, r_P is the z component of the position of the middle bead of the chain $P = N/2$ (measured from the sphere center) and χ the unit cell rotation angle. Note that ϕ_P (azimuthal angle of the subunit P or bond vector \mathbf{u}_P) is fixed in order to remove Goldstone (zero) modes associated with a trivial rotational symmetry around the z axis connecting the sphere center to the middle bead P .

Due to a large number of free variables, we tackle the problem numerically using the quasi-Newton optimization algorithm [61], which locates the minimum of the Hamiltonian using its first-order derivatives. At a minimum, the first-order variation of the Hamiltonian vanishes, i.e.

$$\delta \mathcal{H} = \sum_{i=1}^N \left(\frac{d\mathcal{H}}{d\theta_i} \delta \theta_i + \frac{d\mathcal{H}}{d\phi_{i \neq P}} \delta \phi_{i \neq P} \right) + \frac{d\mathcal{H}}{d\chi} \delta \chi + \frac{d\mathcal{H}}{dr_P} \delta r_P = 0. \quad (10)$$

We use a combination of stochastic and parameter quenching methods to make sure that the obtained structures are not meta-stable (local minima). The meta-stable structures have been discussed elsewhere for chain-sphere complexes [54, 56].

3 Salt-induced structural changes of the fiber - unconstrained optimization

In this section, we investigate the dependence of structural properties of the complex fiber on the salt concentration for fixed macroion charge valency $Z = 15$ and fixed total length of chain per unit cell $L_c = 68 \text{ nm}$ (equivalently $N_{bp} = 200$ base pairs of DNA) [24, 28]. The salt concentration C_s is increased from zero up to the physiologically relevant range of 100 mM monovalent salt and beyond (with the inverse screening length spanning the range $\kappa = 0 - 1.1 \text{ nm}^{-1}$). Here we focus on the unconstrained (full) minimization scheme; therefore, the chain length wrapped around the macroion is not fixed and can change accordingly. The results display a variety of helical

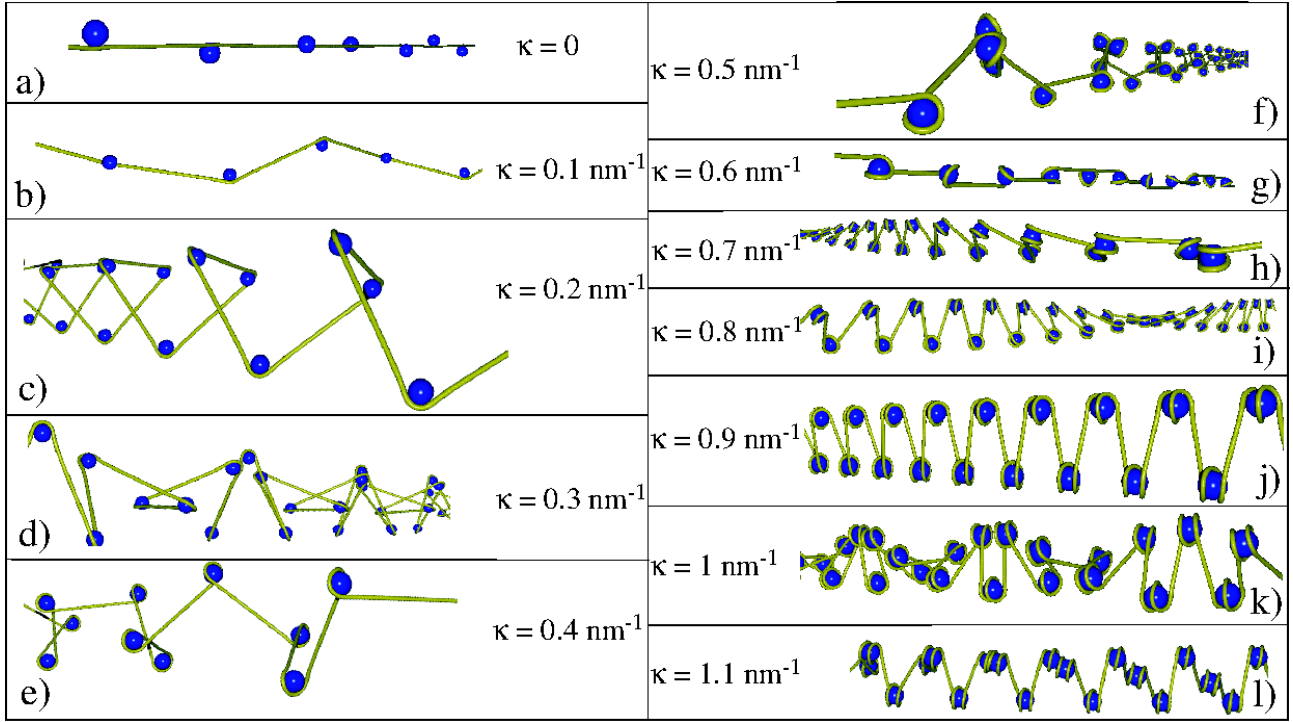


Fig. 2. The optimal spatial configuration of the complex fiber as calculated from the unconstrained minimization of the Hamiltonian Eq. (7) for macroion (sphere) charge valency $Z = 15$, total chain length per unit cell (per sphere) of $L_c = 68$ nm (equivalent to 200 DNA base pairs) and for various Debye inverse screening lengths as indicated on the graph.

fibers as visualized in Fig. 2, which reflect drastic structural variations by changing the salt concentration.

The ground-state configurations shown in the Figure can be grouped into a few generic classes, such as *beads-on-a-string* (Figs. 2a, b, g), *zig-zag* or *cross-linker* (Figs. 2d, h-l) and *loose solenoidal structures* (Figs. 2c, e, f). These types of patterns have been identified more specifically within recent geometric models for the chromatin fiber [18, 27, 35]. In general, the zig-zag pattern can be thought of as a configuration in which successive core particles are located on opposite sides of the fiber and the straight linker chain joining them bridges across the helical core of the fiber. This property is absent in the loose solenoidal pattern where successive nucleosomes are adjacent (as nearest neighbors). Note that this classification is only qualitative in the present context and will be used for convenience when referring to the structures obtained from our model. A more quantitative analysis of the salt-dependent behavior will be discussed in the following Sections.

As seen, the degree of chain complexation increases with increasing salt concentration. The highly wrapped states occur at intermediate salt concentration and result from the growing dominance of electrostatic chain-sphere attraction against the chain (electrostatic and bending) self-energy. Indeed, as we show later, macroions are highly *overcharged* by the PE adsorption much in the same way as a single isolated complex is overcharged at intermediate to large salt concentration [54, 55, 62, 63].

At vanishing salt concentration (Fig. 2a), the PE chain takes a straight-line shape due to the dominant electrostatic self-energy of the PE chain as charged units interact with long-ranged (unscreened) Coulomb interaction. The distribution of spheres around the chain is periodic but their centers lie on different angular locations around the chain. For inverse screening length in the range of $\kappa = 0.3$ to 0.6 nm⁻¹ (Figs. 2d-g), the fiber structure shows an anomalous behavior, i.e., the diameter of the fiber decreases and the projected distance (along the fiber axis) between neighboring sphere centers increases, which is due to the fact that the chain strand completes its first turn around each sphere (see also Fig. 3). Upon further complexation of the chain (Figs. 2h-l), the fiber thickness tends to increase again and the spheres become more densely packed. Note that in the range of Debye inverse screening lengths $\kappa = 0 - 0.5$ nm⁻¹ (<25 mM monovalent salt), the chain wrapping is less than a complete turn and these configurations appear locally as beads-on-a-string structures. However, the chain wrapping may be increased by taking a higher sphere charge, leading to different structures even for small κ , as shown elsewhere [56]. The role of sphere charge will be discussed later.

3.1 Overcharging of the core particle

It is useful to consider the local structure of the core particles within the fiber in more detail. A closer view of the unit cell of the fiber is shown in Fig. 3 for different salt

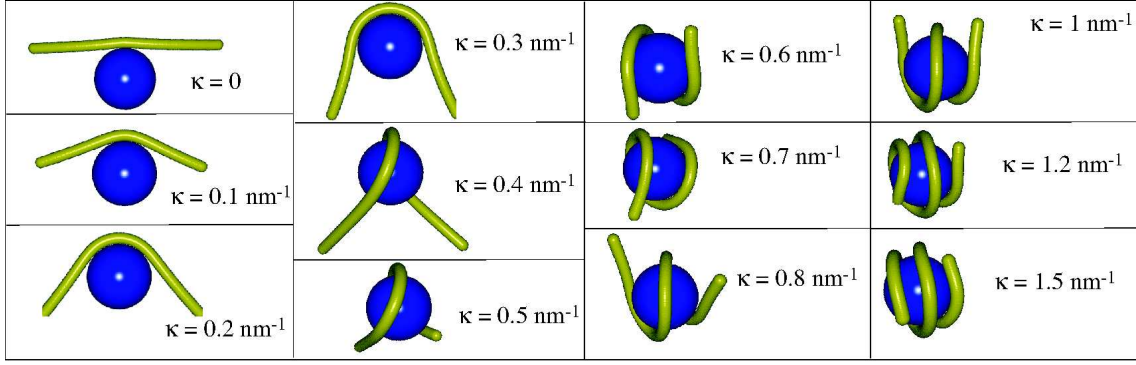


Fig. 3. The local shape of the core particles within the optimal fiber structures in Fig. 2 for sphere charge valency $Z = 15$ and various Debye inverse screening lengths as indicated on the graph. The total length of the PE chain per unit cell is fixed as $L_c = 68$ nm ($N_{bp} = 200$). The increase in the number of chain turns around the macroion is clearly demonstrated.

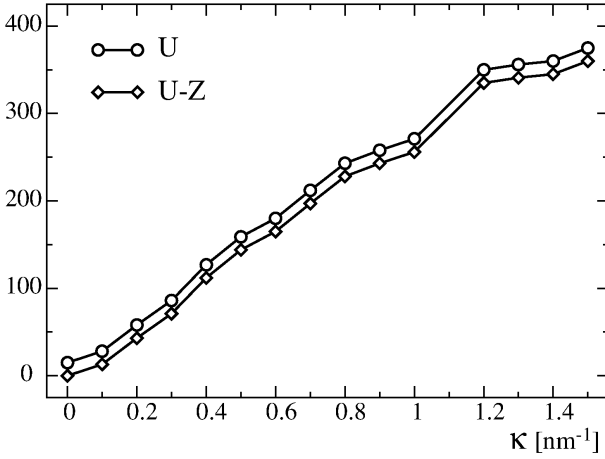


Fig. 4. Number of chain beads (circles) that are attached to the sphere (i.e., within the distance $1.02R_s$ from the sphere center where $R_s = 5$ nm is the sphere radius) as a function of the inverse screening length for the structures shown in Figs. 2 and 3. As noted before each bead is monovalent ($q = 1$), thus this number equals the PE charge adsorbed on the sphere. Diamonds show the net charge of the complex. At very low salt concentration, the sphere charge is already nearly compensated by the adsorbed PE segment and for larger salt, the sphere is strongly overcharged.

concentrations. We introduce two quantities that measure the degree of PE chain wrapping around each macroion in the fiber, namely, the *adsorbed* PE charge, U (that includes only those chain beads that are within distances less than or equal to $1.02R_s$ from the sphere center), and the net charge of the core particle defined as $U - Z$. Both quantities are shown in Fig. 4 as a function of κ .

The unit cell configurations clearly show that the PE chain becomes gradually more wrapped around the sphere upon increasing the salt concentration. That amounts to more than two complete turns at high salt ($\kappa = 1.5$ nm⁻¹). As seen from Fig. 4, the adsorbed PE charge increases

almost linearly with the salt concentration and reaches a plateau-like region at high salt in agreement with the behavior observed for a single isolated complex [56]. The saturation at high salt is due to the finite and fixed length of the PE chain per sphere that is 200 DNA base pairs in the present case. The adsorbed PE charge amounts to that of a DNA segment of 146 base pairs at about the physiological salt concentration ($\kappa \simeq 1$ nm⁻¹) [54].

Note that for the chosen parameters here (with sphere valency of $Z = 15$), the core particle is always overcharged, that is $U - Z > 0$. The overcharging degree, $(U - Z)/Z$, becomes quite large at intermediate salt, such that the net complex charge becomes more than twenty times larger in magnitude than the bare sphere charge. This striking feature is known to occur due to strong lateral chain segment correlations at large salt concentration, which leads to a highly ordered adsorbed layer on the macroion surface [54, 55, 62, 63, 64]. In this situation, the spacing between chain strands on the sphere is of the order of the Debye screening length, κ^{-1} [64].

The unit cell configurations in Fig. 3 also display how the relative entry-exit angle of the chain in a core particle is influenced by the changes in the salt concentration. The changes in the relative entry-exit angle in turn affects the overall arrangement of the core particles and thus the global structure of the fiber as seen in Fig. 2.

3.2 Geometry of the fiber

Besides the overall shape, one is interested in geometrical characteristics of the fiber and the way they vary with the salt concentration. Here we consider the following parameters (see Fig. 5):

- The fiber diameter, D_F , which refers to the diameter of the smallest *outer* cylinder coaxially enclosing the fiber.
- The projected center-to-center distance, $d_{||}$, of consecutive spheres along the central fiber axis, which gives a measure of *projected density* of the fiber, $n_{||}$; conventionally, we represent the fiber density as the number

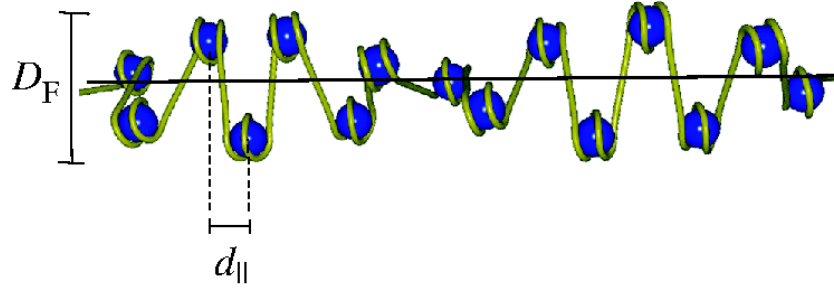


Fig. 5. Schematic representation of the fiber diameter, D_F , and the projected center-to-center distance, $d_{||}$, of consecutive spheres along the fiber axis. The central fiber axis is shown by a horizontal solid line.

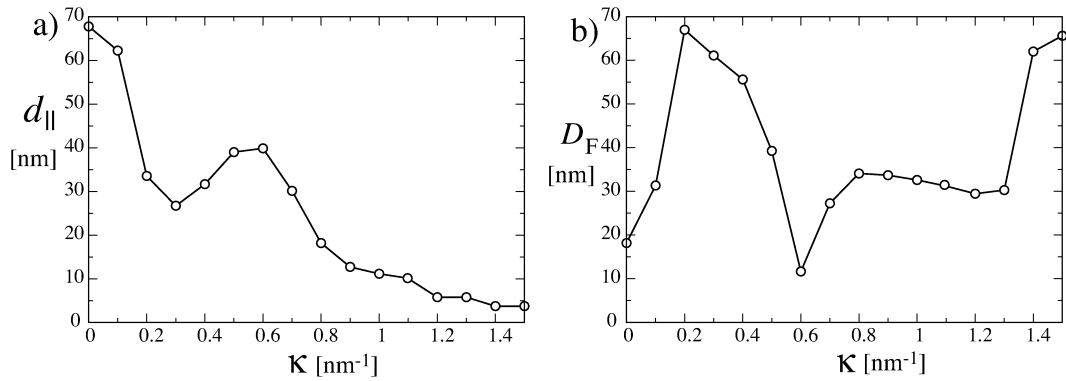


Fig. 6. a) The projected distance of neighboring sphere centers along the fiber axis, $d_{||}$, and b) the fiber diameter, D_F , as a function of the inverse screening length. The macroion charge and chain length per unit cell are fixed as $Z = 15$ and $L_c = 68$ nm.

of spheres per 11 nm as typically expressed in experimental literature for chromatin [28]; i.e.

$$n_{||} = \frac{11}{d_{||}}, \quad (11)$$

where $d_{||}$ is measured in units of nm.

- The entry-exit angle, ψ , and the dihedral angle, ξ , which can be defined (Section 4) in analogy with the chromatin models [27] (see Fig. 7).

As seen in Fig. 6a, the projected distance takes a maximum value of about $d_{||} = 68$ nm at zero salt concentration and then falls off in a non-monotonic fashion to quite small values of about sphere radius $d_{||} \simeq R_s = 5$ nm, when the inverse screening length (salt concentration) exceeds $\kappa = 1 \text{ nm}^{-1}$ (100 mM NaCl) representing a dense fiber of a density about $n_{||} = 2$. The projected distance displays a local minimum and a local maximum at inverse screening lengths of about $\kappa = 0.3 \text{ nm}^{-1}$ and $\kappa = 0.6 \text{ nm}^{-1}$, respectively. These extrema roughly correspond to extrema in the fiber diameter, D_F , which shows an almost opposite trend as compared with the projected distance when the salt concentration is varied (Fig. 6b). At zero salt, the outer fiber diameter is roughly twice the sphere diameter, i.e., $D_F = 20$ nm, due to a staggered configuration of the spheres. It changes rapidly at small salt concen-

tration with κ , reaching a maximum and then a sharp minimum at an intermediate salt concentration of about $\kappa = 0.6 \text{ nm}^{-1}$, where the projected distance exhibits a local maximum. The minimum fiber diameter at this point is about 10 nm (equal to the sphere diameter); hence at $\kappa = 0.6 \text{ nm}^{-1}$, the complex fiber shows its largest projected distance to diameter ratio $d_{||}/D_F = 4$, reflecting an almost one-dimensional beads-on-a-string structure (see Fig. 2g).

Interestingly, over the range of intermediate salt concentrations between $\kappa = 0.8$ and 1.3 nm^{-1} (corresponding to 60-160 mM monovalent salt), the fiber diameter remains almost unchanged at about $D_F = 30$ nm (reflected by a plateau-like region in Fig. 6b), although the fiber structure changes from the zig-zag to loose solenoidal pattern (see also Fig. 8). The chain wrapping in this region amounts to about 1-and-3/4 turn, close to that in the nucleosome core particles in chromatin at intermediate salt concentration about the physiological regime [16, 24, 27, 28]. In fact, the experiments reveal that the chromatin fiber exhibits a dense structure in this regime with a diameter of about 30 nm, the so-called “30 nm fiber”. The present results, which predict a stable 30 nm complex fiber at intermediate salt concentration, thus appear to give a trend consistent with those found in chromatin experiments [16, 24, 27, 28]. The present full-minimization

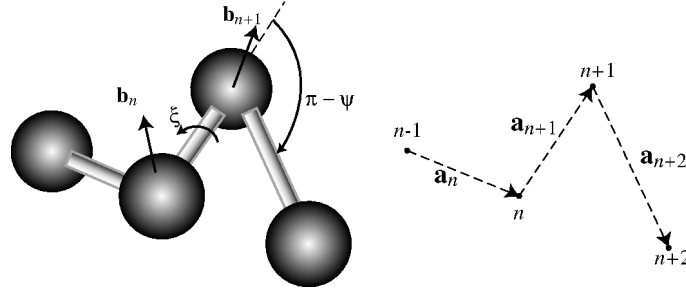


Fig. 7. A schematic view of the two-angle representation of macroion positions along the chromatin fiber. Each two successive spherical macroions, labeled by $n - 1$ and n , are connected to each other via a vector \mathbf{a}_n . The entry-exit angle ψ is defined as the complementary angle between any two consecutive connecting vectors (shown in the figure for \mathbf{a}_{n+1} and \mathbf{a}_{n+2}), which is the same for all n in a homogeneous helical structure as is the case in the present model. On the other hand, each three successive macroions (e.g., those labeled by $n - 1$, n and $n + 1$) define a plane with a normal vector $\mathbf{b}_n = \mathbf{a}_n \times \mathbf{a}_{n+1}$. The dihedral angle ξ is defined as the angle between two such normal vectors (shown in the figure for \mathbf{b}_n and \mathbf{b}_{n+1}).

model however is very different from the H1-stabilized chromatin because (aside from other realistic factors in chromatin that are missing in our model) the structure of the core particle (and the conformation of the entering and exiting chain strands) can change subject to interactions with other units. Thus the local fiber structure is different from that of chromatin. We also obtain a lower density of spheres ($n_{||} \leq 1$) as compared with the chromatin fiber. The present results however suggest that such 30 nm fibers may be feasible in mixtures containing DNA and synthetic nano-colloids at intermediate salt concentrations.

For large salt concentrations (beyond $\kappa = 1.3 \text{ nm}^{-1}$), the fiber diameter rapidly increases but the projected distance between spheres remains constant. At $\kappa = 1.5 \text{ nm}^{-1}$, the fiber exhibits a small ratio of $d_{||}/D_F = 0.077$, corresponding to a tight solenoidal shape (shown on Fig. 8).

3.3 Two-angle structural diagram

The arrangement of *macroions* along the fiber within the present model may also be described using a two-angle description in the spirit of the two-angle model presented in Ref. [27] for the chromatin fiber. For the sake of analogy, we define an entry-exit angle, ψ , and a dihedral angle, ξ , as follows (see Fig. 7).

Let us assume that $\mathbf{a}_n = \mathbf{R}^n - \mathbf{R}^{n-1}$ is the connecting vector between two successive macroion centers, where \mathbf{R}^n is the position of the n -th sphere. The entry-exit angle, ψ , is defined from the angle between two such consecutive connecting vectors, \mathbf{a}_n and \mathbf{a}_{n+1} , i.e.

$$\psi = \pi - \cos^{-1} \left(\frac{\mathbf{a}_n \cdot \mathbf{a}_{n+1}}{|\mathbf{a}_n| |\mathbf{a}_{n+1}|} \right). \quad (12)$$

The dihedral angle, ξ , the angle by which four consecutive spheres are out-plane, is determined by calculating the angle between the normal vectors of two planes, one identified by the spheres \mathbf{R}^{n-1} , \mathbf{R}^n , \mathbf{R}^{n+1} and the other identified by \mathbf{R}^n , \mathbf{R}^{n+1} , \mathbf{R}^{n+2} . Explicitly, one has

$$\xi = \cos^{-1} \left(\frac{\mathbf{b}_n \cdot \mathbf{b}_{n+1}}{|\mathbf{b}_n| |\mathbf{b}_{n+1}|} \right) \quad (13)$$

with $\mathbf{b}_n = \mathbf{a}_n \times \mathbf{a}_{n+1}$. In a homogeneous helical structure, which is the case in the present model, ψ and ξ are independent of n and thus the same angles are obtained between any two consecutive vectors.

By calculating these two angles for various salt concentrations, one can sketch a two-parameter $\xi - \psi$ structural diagram. The result is shown in Fig. 8 for fixed sphere charge $Z = 15$ and fixed chain length (per unit cell) of $N_{bp} = 200$. Open circles give the two-angle coordinates associated with the numerically calculated optimal configuration at given inverse screening lengths (indicated by numbers on the graph).

It follows from the diagram that the angle ψ determines the compactness of the fiber, while ξ roughly determines its structural class, e.g., being zig-zag or solenoidal. At small salt concentrations, these angles vary rapidly with the salt concentration, which, as mentioned above, is a consequence of the chain wrapping process. At high salt, most of the free length of the chain available in a unit cell is already wrapped and thus the angles vary weakly. The parameter which varies more dramatically with κ is ψ . As seen, ψ never becomes smaller than $\pi/4$, due to excluded-volume interactions [18], while ξ spans the whole interval $0 < \xi < \pi$.

The beads-on-a-string patterns are found at the boundaries of the diagram with entry-exit angles roughly in the range $3\pi/4 < \psi < \pi$. While the compact solenoidal structures appear in the lower right corner, that is with small dihedral angle $0 < \xi < \pi/4$ but large entry-exit angle $3\pi/4 < \psi < \pi$. One may thus distinguish *compact solenoidal* structures on the lower-right corner of the graph. The 30 nm zig-zag structures obtained at intermediate salt regime typically appear on the left upper corner of the graph, that is for $\pi/4 < \psi < \pi/2$ and typically for large $\xi > \pi/2$.

4 Constrained optimization model

As noted before, several features of the actual chromatin structure are not accounted for within the present model.

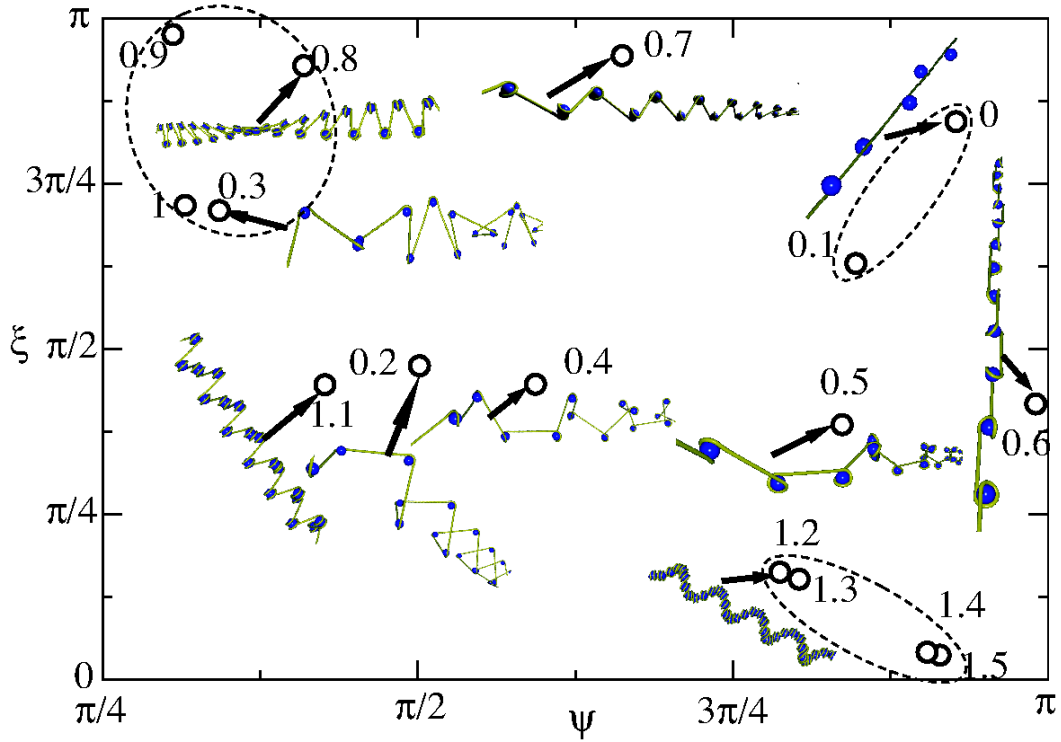


Fig. 8. The two-angle diagram for fiber structures from unconstrained optimization at fixed macroion charge valency $Z = 15$, fixed chain length per unit cell $L_c = 68$ nm ($N_{bp} = 200$), and for various κ . The value of κ associated with each point is indicated on the graph (in units of nm^{-1}). The zig-zag structures (upper left corner), beads-on-a-string structures (upper right region), and compact solenoids (lower right region) are indicated schematically by closed ellipses and for each case a characteristic structure is shown.

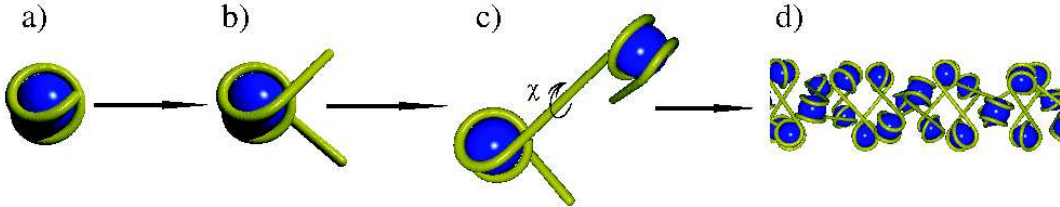


Fig. 9. In the constrained optimization model, the conformation of the chain in each unit cell is fixed and only the rotational angle χ can vary. The core particle complex (a) consists of a chain segment of length equivalent to 146 DNA base pairs, whose configuration is obtained from numerical minimization of a single isolated complex for a given sphere charge and salt concentration. The core particles are linked together with straight linker chain of arbitrary length (b) (in the shown configuration, the total chain length per unit cell is $N_{bp} = 200$). The replication procedure (c and d) is the same as explained in Section 2.2.

One factor is the so-called *linker histone* H1, a cationic protein which binds near the entry-exit region of the DNA in the nucleosome. It brings together the two strands of the DNA that enter and exit the central core particle forming a stem-like pattern [24, 28]. In *in vitro* experiments, H1 histone can be removed by exposing the system to high salt concentrations (about 0.6 M), and washing the solution in order to remove dissociated linker histone. In such H1-depleted cases, the chromatin fiber appears to be rather open and loose (i.e., with a low number of histones per unit length along the fiber) [24]. While in the experiments with H1-stabilized linker histone, the core particle config-

uration is fixed and no unwrapping of the DNA on the histone octamer is possible [28]. As a result, the number of base pairs complexed with the histone octamer is fixed.

Motivated by this observation, we introduce a variant of the preceding model, in which the structure of the core chain-sphere complex is constrained to be fixed. At any given value of the macroion charge Z and the inverse screening length κ , we fix the core structure within each unit cell according to the optimal (ground-state) configuration of an *isolated* complex (with a total chain segment of length about 146 DNA base pairs). This structure is obtained from a similar minimization study as discussed

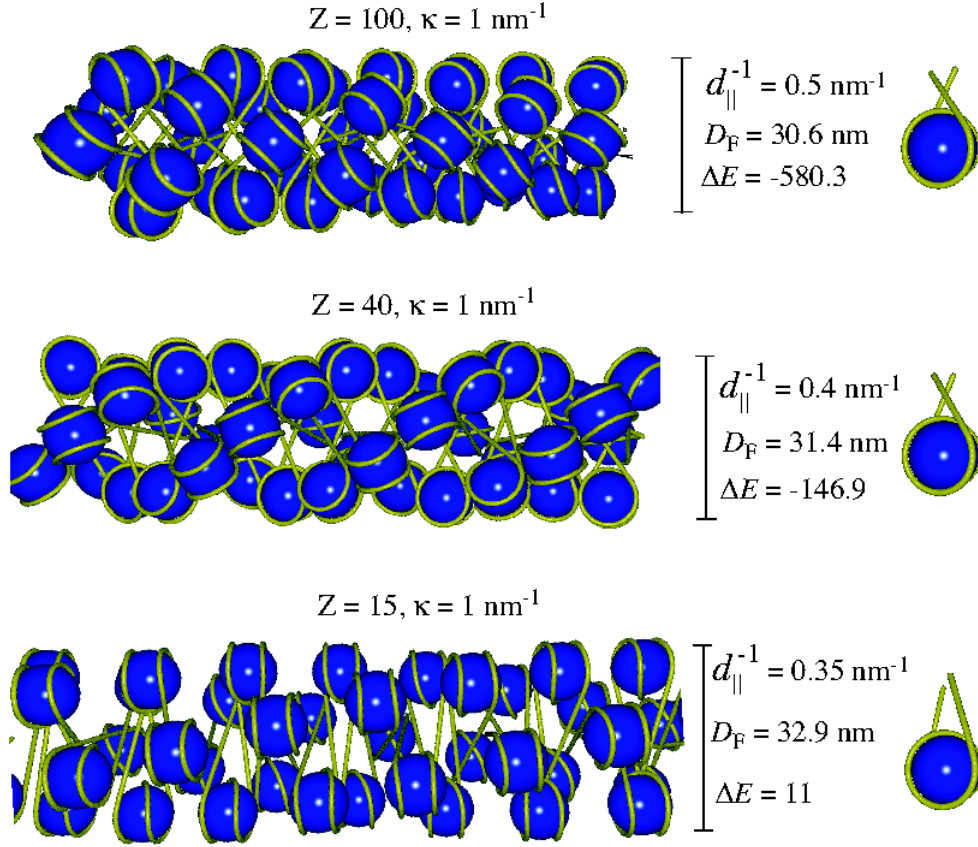


Fig. 10. Optimal fiber configurations obtained from the constrained optimization model for different sphere charge Z as indicated on the graph but for fixed inverse screening length $\kappa = 1 \text{ nm}^{-1}$ and PE chain length per unit cell $N_{bp} = 200$. The inverse projected distance, d_{\parallel}^{-1} , the binding energy, ΔE (in units of $k_B T$), and the fiber diameter D_F are given in the graph for each fiber. The corresponding local structure of the fiber unit cell is shown on the right.

in Refs. [54,55]. We then connect straight linker chains of arbitrary length to the strands of the chain entering and exiting the core particle. This constitutes a single unit cell for the fiber which is hence constructed by replicating this unit cell using the transformation method explained in Section 2.2—see Fig. 9. Note, however, that in this case, there is only *one* degree of freedom, that is the angle χ , which can be varied in order to find the minimum of the effective Hamiltonian of the fiber (see Sections 2.3 and 2.4). Note also that the entry-exit angle is dictated by the configuration of a single complex in *isolation*, which thus depends only on the sphere charge, Z , and the salt concentration via κ , but not on the linker length.

4.1 Optimal constrained configurations for various sphere charge

In Fig. 10, we show several structures obtained from the constrained minimization for the inverse screening length $\kappa = 1 \text{ nm}^{-1}$ and for large to small sphere charge Z (at fixed chain length $N_{bp} = 200$). It is seen that the compactness of the fiber is less sensitive to changes in the sphere

charge. As a result, the entry-exit angle of the PE strand changes weakly as compared with the unconstrained minimization case. The fiber becomes denser for large sphere charge: For $Z = 15$, we have $d_{\parallel}^{-1} = 0.35 \text{ nm}^{-1}$ corresponding to $n_{\parallel} = 3.85$ spheres per 11 nm length along the fiber axis, while for $Z = 100$, we have $n_{\parallel} = 5.5$ ($d_{\parallel}^{-1} = 0.5 \text{ nm}^{-1}$), very close to the experimental chromatin value of about 5-6 histones per 11 nm as reported in Refs. [24,26,27,28,29].

In order to understand the underlying mechanism behind the compaction of the fiber with increasing the sphere charge, we consider the binding energy of the fiber, ΔE , i.e., the energy of the optimal configuration measured with respect to the reference state of a free straight PE chain in the absence of attached spheres. While for $Z = 15$, the binding energy is positive (which reflects the fact that we are performing a constrained optimization which does not necessarily find the global energy minimum), it becomes highly negative for larger Z as indicated in Fig. 10, i.e., $\Delta E = -580.3$ (in units of $k_B T$) for $Z = 100$. This in fact reflects effective attractive interactions between core particle complexes within the fiber, which result from correla-

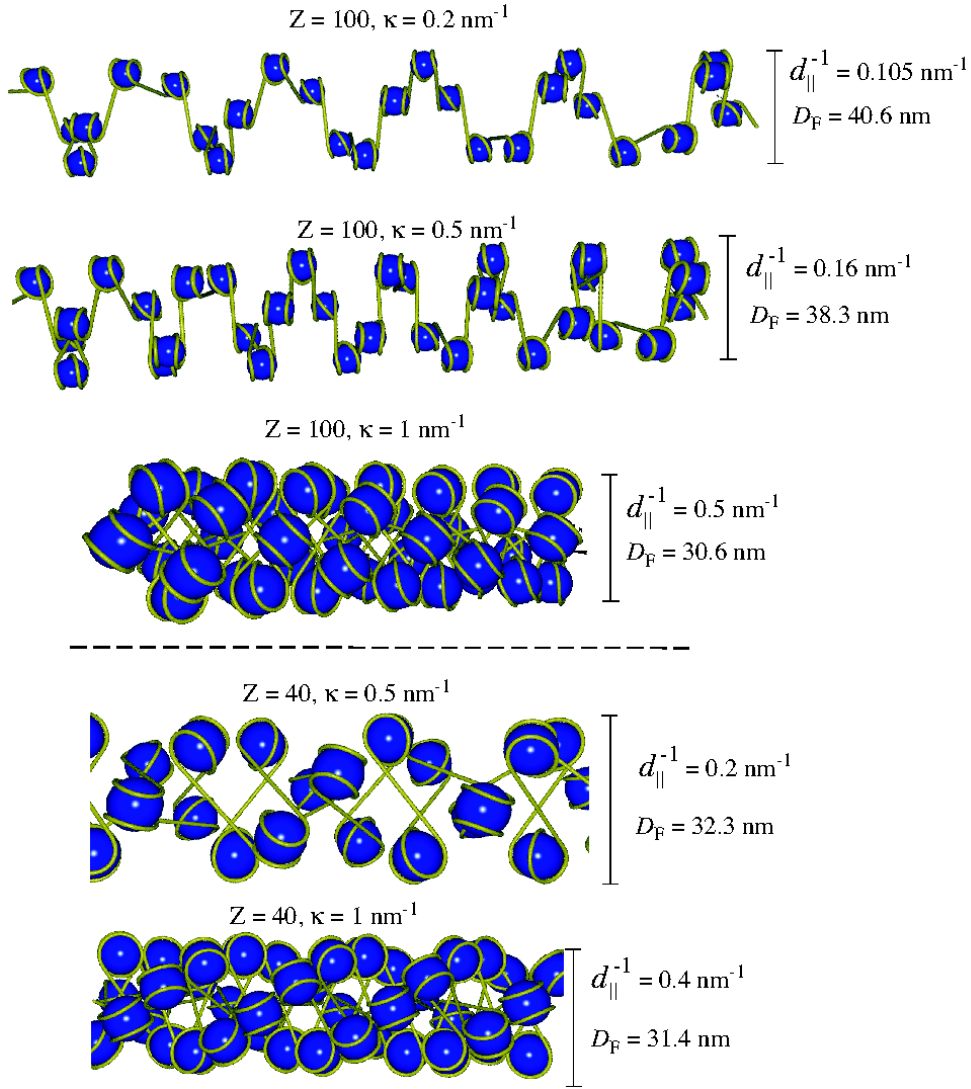


Fig. 11. Same as Fig. 10 but for fixed sphere charge $Z = 100$ and 40 and different inverse screening lengths as indicated on the graph.

tions between positive and negative patches on neighboring core complexes as may be seen in the spatial configurations. Such inter-complex correlations have been studied before [55].

Note also that the diameter of the fiber is quite stable at about $D_F = 30 \text{ nm}$, that is about the diameter of the H1-intact 30 nm chromatin fiber in the physiological salt regime (i.e., $\kappa \simeq 1 \text{ nm}^{-1}$). In fact, the striking point here is that within this simple model, the entering and exiting strands of the PE chain form a cross pattern as explicitly shown by focusing on a single unit cell in Fig. 10 (shown on the right). This situation—that resembles the experimentally observed stem-like pattern for the DNA in the nucleosome—is only obtained within the constrained minimization and leads to a small entry-exit angle, and hence a rather compact fiber in qualitative agreement with the Woodcock model [27].

4.2 Optimal constrained configurations for various salt concentration

In Fig. 11, we show configurations at fixed Z and different salt concentrations. As seen for $Z = 100$, the structure of the fiber becomes expanded for small κ as a direct consequence of the increased electrostatic repulsion between the spheres. The density of the fiber reduces to about one sphere per 11 nm and the fiber diameter increases to about 40 nm as indicated on the graph.

As discussed elsewhere [54, 55], the sphere charge should be taken as an effective (or fitting) parameter within the present model, because the true sphere charge is regulated under experimental condition depending on the pH , or it may shift from the bare value due to charge renormalization effects in a salt solution [58]. In fact, within the present model, the most relevant fiber configurations (that might resemble the chromatin fiber best) are obtained by

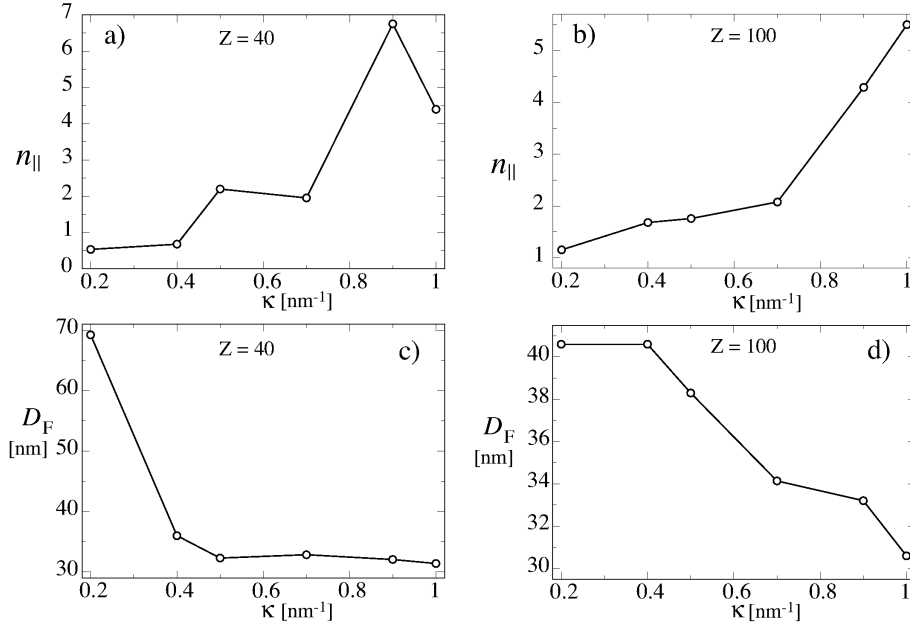


Fig. 12. a) and b) Density of spheres (number of spheres per 11nm along the fiber axis) $n_{||}$, and c) and d) the fiber diameter, D_F , as a function of the inverse screening length as obtained from the constrained optimization model. The macroion charge is $Z = 40$ for a) and c) and $Z = 100$ for b) and d). The chain length per unit cell is fixed at 200 DNA base pairs ($L_c = 68$ nm).

changing Z according to the salt concentration. This may be thought of as a fitting procedure, since as explained above, the effective sphere charge is expected to depend on κ . To make this point clear, note that for instance the fiber configurations for $Z = 100$ and low κ do not show zig-zag patterns [24, 25, 28, 27, 29]. But zig-zag patterns at small κ may be recovered by taking a smaller value for the sphere charge Z (compare $\kappa = 0.5$ nm⁻¹ for $Z = 40$ and 100 in the Figure).

To summarize these results, we plot the the fiber diameter, D_F , and the fiber sphere density, $n_{||}$, in Fig. 12 for two different values of sphere charge $Z = 40$ and 100. Qualitatively, it appears that the sphere density increases from about one at low salt up to 5-6 spheres in the physiological regime of $\kappa \simeq 1.0$ nm⁻¹ (100mM monovalent salt) [18, 24, 26, 27, 28, 29]. Examining the fiber diameter in Figs. 12c and d, we find that the fiber diameter decreases down to almost exactly 30 nm at the physiological regime. It is noteworthy that the arrangement of the spheres in the resultant 30 nm fiber shows a clear double helix pattern for $Z = 40$ and $\kappa = 1$ nm⁻¹.

5 Variation of the chain length - unconstrained optimization

In this Section, we return to the unconstrained optimization model and address the effects due to changes in the length of the PE chain per unit cell, N_{bp} , on the fiber structure. We change N_{bp} in the range of 50 to 240 DNA base pairs and focus on the inverse Debye screening length

$\kappa = 0.8$ nm⁻¹ and the sphere charge valency $Z = 15$. At this salt concentration, the fiber exhibits a 30 nm zig-zag pattern (Fig. 2) [56].

5.1 Two-angle structural diagram

In Fig. 13, we have sketched a two-angle diagram in terms of the entry-exit angle, ψ , and the dihedral angle, ξ , summarizing the structural changes of the fiber with the chain length per unit cell, N_{bp} (indicated by numbers on the graph). As seen, the optimal configurations are mostly gathered in the boundaries of the graph (unlike the behavior found for varying salt concentration in Fig. 8).

The global features may be summarized as follows. For relatively large chain length per unit cell, the overall structure changes weakly with the length and exhibits, for the parameters chosen here, the zig-zag pattern (upper left corner with large dihedral angles typically $\xi > \pi/2$ and small to intermediate entry-exit angles $\pi/4 < \psi < 5\pi/8$). This is because the structure of the core particle is nearly independent of the chain length in this regime. Note that for $N_{bp} > 200$, almost 120 base pairs of the PE chain are adsorbed on each sphere, and the rest serves as the linker chain. As the chain length decreases down to the length adsorbed on the sphere, i.e., $N_{bp} = 120$, the diameter of the zig-zag fiber reduces to that of the spheres displaying a compact 10 nm fiber with a beads-on-a-string structure (upper right corner with $\psi > 3\pi/4$ and $\xi > 3\pi/4$). For smaller chain lengths, there is practically no linker chain present and the core particles will thus be located very close to each other. There is a narrow range of chain

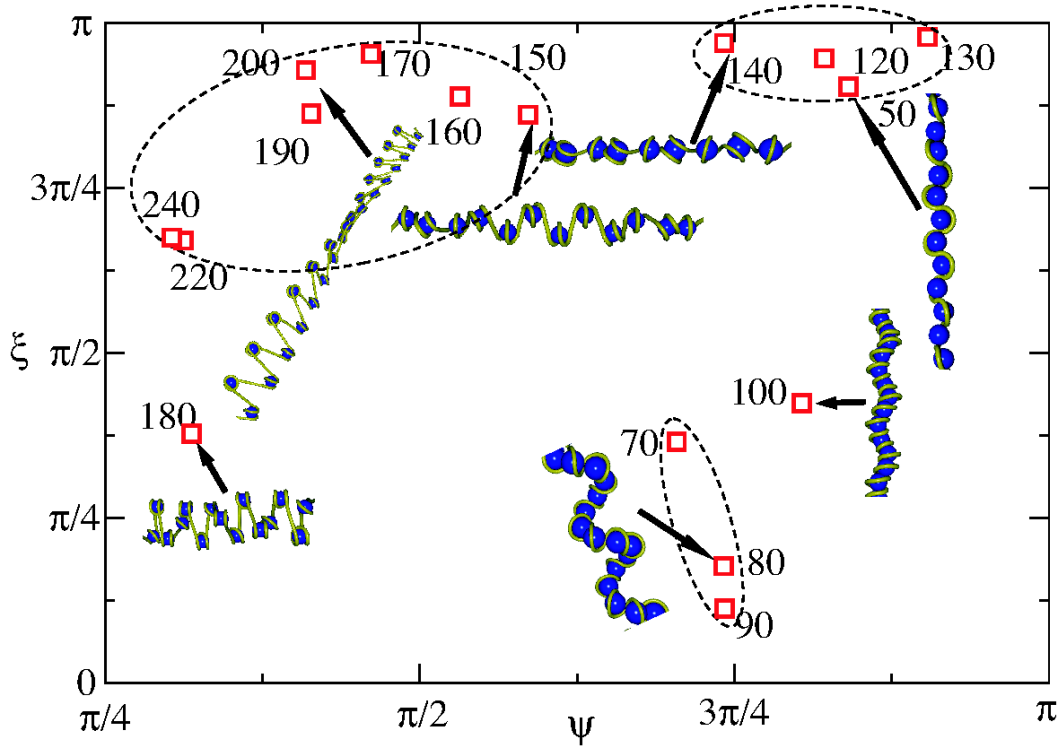


Fig. 13. Entry-exit and dihedral angles diagram for various chain lengths per macroion from unconstrained minimization. The corresponding values of N_{bp} are indicated on the graph. The zig-zag region (top left), beads-on-a-string region (top right) and compact solenoidal region (bottom right) are shown by closed ellipses. Here $\kappa = 0.8 \text{ nm}^{-1}$ and $Z = 15$ are fixed.

lengths $50 < N_{bp} < 100$, where the fiber adopts a compact solenoidal form, with $0 < \xi < \pi/2$ and ψ being distributed around $3\pi/4$. Note that the transition between zig-zag and beads-on-a-string structures involves an increasing entry-exit angle ψ which maximizes the distance between adjacent spheres (minimizing their repulsion), while ξ changes only weakly. In contrast, the transition between beads-on-a-string and compact solenoidal structures involves larger variations in ξ . The isolated zig-zag pattern with chain length $N_{bp} = 180$ corresponds to a local minimum in the binding energy of the fiber as will be discussed below.

5.2 Energetic evidence for intra-fiber phase separation

In the preceding Section, we discussed configurational variations associated with changes of the length of the PE segment per unit cell. Now we turn to thermodynamics and assume that we have a solution of an infinitely long polyelectrolyte and oppositely charged spherical macroions. In this case, an interesting question is one of the equilibrium state of the system. In other words, what would be the resultant linear number density of macroions attached to the polyelectrolyte chain and the fiber structure? Clearly, a complete answer to this question requires a full thermodynamic study by considering the free energy in an appropriate ensemble. But within the ground-state-dominance approximation, one can address this question *on the energetic level*, i.e., neglecting entropic effects.

In order to investigate the stability of the system, we calculate the fiber binding energy, $\Delta E = \mathcal{H} - \mathcal{H}_0$, where the first term is the energy of the complex fiber, defined in Eq. (7), and the second term is the energy of a free straight PE chain in the absence of attached spheres, which is used as reference. Note that ΔE , \mathcal{H} and \mathcal{H}_0 are energies per unit cell and in units of $k_B T$. One can then envision two different ensembles: An ensemble consisting of a *fixed* number of macroions adsorbed on a *fixed* large length of the PE chain (ensemble A), and an ensemble consisting of macroions adsorbed from a bulk reservoir (with a fixed chemical potential) on a *fixed* large length of the PE chain (ensemble B).

Ensemble A is realized in a situation where the total number of macroions is finite and thus macroions are depleted from the solution, and where the total length of DNA available for adsorption is fixed such that the mean linear concentration of adsorbed macroions is finite and can be treated as an input parameter. To study thermodynamic equilibrium, in this case one has to consider the binding energy per unit cell or sphere as a function of the chain length per unit cell, N_{bp} . This is shown in Fig. 15a for fixed $\kappa = 0.8 \text{ nm}^{-1}$ and $Z = 15$. As seen, ΔE appears to have two minima at intermediate values of N_{bp} , i.e., one at about $N_{bp} = 100$, where the fiber exhibits a compact solenoidal structure, and the other minimum at about $N_{bp} = 120$, where a compact beads-on-a-string structure is obtained as discussed before. Also ΔE shows an over-

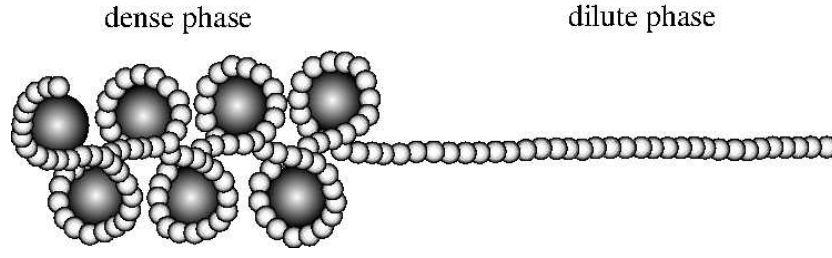


Fig. 14. Schematic view of the ensemble A with fixed number of macroions adsorbed on a fixed length of the PE chain, exhibiting phase-coexistence between a dense and a dilute phase.

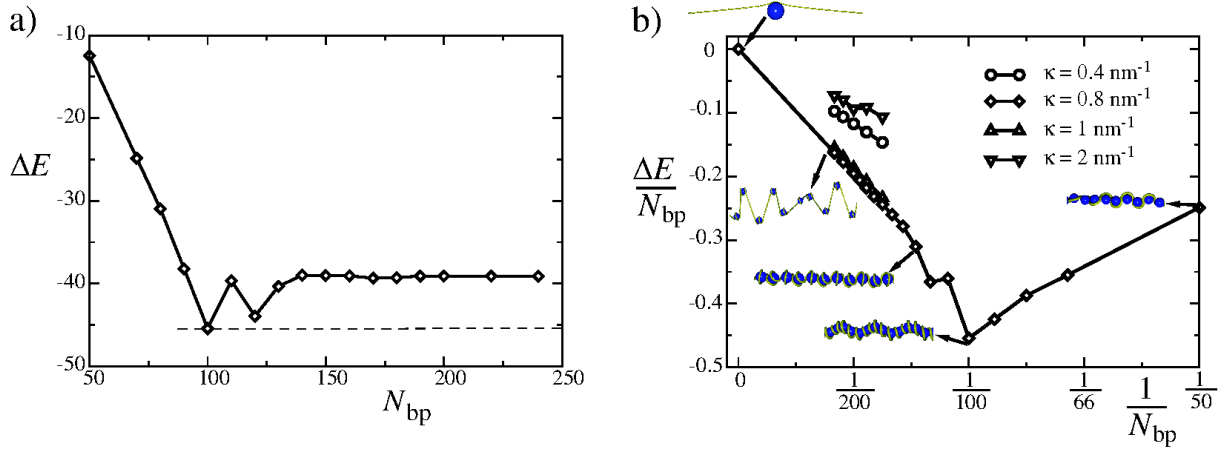


Fig. 15. a) Binding energy of the complex fiber (per unit cell and in units of $k_B T$) as a function of the chain length per unit cell N_{bp} and b) the binding energy per chain unit length as a function of the concentration of adsorbed macroions on the chain, $1/N_{bp}$, for different values of κ as indicated in the graph.

all non-convex behavior between $N_{bp} = 100$ and the limit of an infinitely dilute fiber (with no macroion adsorbed), i.e., $N_{bp} \rightarrow \infty$. Thermodynamic stability follows from the standard common-tangent construction (indicated by the broken line in Fig. 15a), which indicates a gas-liquid-type “phase coexistence” along the fiber between a liquid phase of high sphere concentration and a gas phase of vanishing sphere concentration (see Fig. 14). In between, the energy has a non-monotonic behavior with values higher than the common-tangent line, which thus represents a region of meta-stable structures. Adding the one-dimensional translational entropy of adsorbed macroions would lead to a dilute gas phase with a finite sphere density. Note that we do not consider the possibility of a higher density of spheres on the chain (i.e. a smaller number N_{bp} of base pairs per unit cell) than corresponding to the minimum in energy in Fig. 15a.

In the case of ensemble B, one deals with a complex fiber in equilibrium with a reservoir of macroions, where the density of macroions on the chain is controlled by the chemical potential of macroions in bulk solution. To study thermodynamic equilibrium in this case, one has to consider the binding energy per unit length of the PE chain $\Delta E/N_{bp} = \mathcal{H}/N_{bp} - \mathcal{H}_0/N_{bp}$ as a function of the adsorbed macroion density along the chain, $1/N_{bp}$, which is shown

in Fig. 15b for fixed $\kappa = 0.8 \text{ nm}^{-1}$ and $Z = 15$. We also show data for $\kappa = 0.4, 1$ and 2 nm^{-1} for large N_{bp} . Note that the data corresponding to $\kappa = 0.8 \text{ nm}^{-1}$ lie below the other data, i.e., for this range of N_{bp} , the energy of optimal fiber is minimal at $\kappa = 0.8 \text{ nm}^{-1}$ as compared to other values of κ [56]. For the data set for $\kappa = 0.8 \text{ nm}^{-1}$, $\Delta E/N_{bp}$ exhibits two minima at intermediate values of macroion density, i.e., one at about $1/N_{bp} = 0.01$ ($N_{bp} = 100$), and the other minimum at about $1/N_{bp} = 0.008$ ($N_{bp} = 120$). Note that the location of the minima of $\Delta E/N_{bp}$ are in principle different from the minima of ΔE , but the relative shift is rather negligible. Phase coexistence between two fiber phases of different densities in this ensemble would correspond in fact to three phase coexistence, i.e. matching chemical potentials in the two fiber phases and in the bulk macroion solution, and will thus be rather unlikely since it only occurs when the bulk chemical potential exactly matches the chemical potentials of the dense and dilute phases simultaneously. In most cases, the equilibrium will thus consist of a single phase with a macroion density corresponding to the minimum of the energy density in Fig. 15b. If the number of spheres in solution is less than needed to homogeneously populate the chain, one crosses over to ensemble A with a fixed sphere density which is less than the optimal state of ensemble B.

6 Conclusion and discussion

In this paper, we present a systematic numerical approach for investigating the structural properties and energetic stability of complex fibers formed by complexation of a long, semi-flexible polyelectrolyte chain with many oppositely charged spheres. The complex fiber is described using a chain-sphere cell model, in which the detailed structure of the PE chain (locally wrapped around individual spheres) as well as interactions between various components (chain segments and spheres) are taken into account. These interactions include salt-screened electrostatic interactions between all charged units (using linear Debye-Hückel potential), the bending elasticity of the PE chain as well as the excluded-volume interactions between the PE chain and spheres. Here we choose parameters consistent with the DNA-histone system (e.g., using the DNA charge and persistence length and a hard-core sphere radius of 5 nm), but vary the salt concentration, sphere charge, and chain length per sphere as control parameters.

We focus on the optimal structure of the fiber, i.e., the structure which minimizes the effective Hamiltonian of the system for a given set of parameters. This amounts to a ground-state analysis, which is expected to be valid for strongly coupled complexes (large polymer adsorption energy and relatively small thermal fluctuations) [54, 55]. Two different schemes are used here for the optimization procedure: i) unconstrained optimization, and ii) constrained optimization. In the former case, we treat the positions of all chain beads within a fiber unit cell as degrees of freedom in addition to an independent degree of freedom that defines rotational orientation of two adjacent unit cells (core particles) with respect to each other. This case therefore requires a many-variable optimization analysis. In the other case, the conformation of the PE chain on each macroion sphere is fixed according to the optimal configuration of a single isolated PE-macroion complex. Two such complexes are then linked one by one to form a fiber with the help of straight linker chains and the only degree of freedom in this case is the relative rotation of unit cells around the linker chain. In both cases, a variety of helical structures are obtained for the fiber including, in particular, the zig-zag patterns. There are however qualitative differences between the two models.

In unconstrained minimization, the PE conformation is free to change on the sphere, i.e., upon changing the salt concentration or the macroion charge, the PE chain in each core complex may become increasingly more wrapped or unwrapped. As a result, the entry-exit angle of the PE strand varies accordingly, leading to dramatic changes in the overall fiber structure. As shown, the optimal fiber structure shows beads-on-a-string pattern or thick and loose solenoidal patterns at low salt. At about the inverse screening length $\kappa = 0.6 \text{ nm}^{-1}$, the chain is already wrapped around the sphere for almost a complete turn. In this case, the spheres are aligned and form a fiber of diameter about 10 nm, which to some extent resembles the swollen 10 nm beads-on-a-string chromatin fiber. For salt concentrations within the physiological regime, zig-zag patterns are found as optimal structures and the fiber

diameter is about 30 nm; this diameter and the fact that the fiber structure is zig-zag in the physiological regime thus appear to agree with those proposed for chromatin in Refs. [24, 25, 26, 27, 28, 29], although the present model predicts a qualitatively different core particle structure. This is because the linker histone (absent in the present model) plays a key role in the compaction of chromatin into a 30 nm fiber by gluing together the entering and exiting strands of the DNA and thus sealing off the internal structure of the DNA in the nucleosome core particle. In our unconstrained model, the entering and exiting strands of the chain are displaced and divergent and thus, the density of spheres along the fiber appears to be much smaller (i.e., about one sphere per 11 nm along the fiber axis) than the value proposed in the cross-linker models (about 5-6 spheres per 11 nm [18, 24, 26, 27, 28, 29]). For higher salt concentrations, the chain wrapping degree still increases and the spheres become highly packed along the fiber backbone (for fixed chain length per sphere), leading to compact solenoidal structures.

We have also studied the role of sphere charge and chain length per sphere and their influence on the fiber structure. An important result is that when the chain (linker) length per macroion is treated as a free parameter, the binding energy (per sphere or unit cell) is found to take a non-convex shape at intermediate salt concentrations when plotted as a function of the chain length per sphere. A simple common-tangent construction indicates a gas-liquid-type “phase coexistence” along the fiber, i.e., a part of the PE chain forms a dense complex with macroions phase-separating from a dilute phase along the fiber.

In the constrained optimization model, the core particle structure is fixed and only the relative rotation of the core particles (unit cells) is allowed in order to minimize the fiber Hamiltonian. As shown, for large sphere charge and within the physiological salt regime, the fiber shows zig-zag pattern and sphere densities of about 5-6 spheres per 11 nm length along the fiber axis. Indeed, both the global structure as well as the fiber density and diameter in this case resemble more closely the structures found or proposed for chromatin in Refs. [24, 26, 27, 28, 29]. Interestingly, the dense zig-zag pattern results from the fact that the entering and exiting strands form a cross pattern leading to a small entry-exit angle; the form of the entry-exit strands in this case tends to resemble the stem-like form expected in chromatin in the presence of the linker histone [27, 28] and is therefore found to be a similarly important factor in order to obtain dense fiber structures in our model. The constrained model is thus similar to the two-angle model proposed by Woodcock et al. [27], except that here we employ a realistic interaction potential between the core particles.

We emphasize again that the present results are obtained for a generic charged chain-sphere complex fiber and no direct comparison with the 30 nm chromatin fiber (which involves additional structural and specific details) should be attempted. Especially, the linker histone effects or other factors such as histone tails or the specific shape

of the histone octamer are not incorporated within the present model, and the constrained optimization model is only a simple way to mimic the linker-histone stabilization of the nucleosome. On the other hand, our model and its predictions are applicable to the mixtures of DNA and synthetic oppositely charged spheres and suggest that chromatin-like structures should also be observable in such systems. The main advantage of the present approach is that it accounts for the detailed wrapping state of the PE chain within a fiber as well as the essential intra-fiber interactions, and that it can easily be generalized to more sophisticated models.

In this work, we have also neglected the excluded-volume interaction between chain segments. (Note that the chain-sphere volume interaction and the finite radius of DNA is taken into account via the hard-core radius of the sphere as explained in the text.) The chain-chain excluded-volume interaction is expected to play a role only at high salt concentration (typically beyond 100mM monovalent salt for intermediate sphere charge), where the chain wraps around the spheres more than two turns. (For a complete analysis and possible improvements of the basic chain-sphere scheme used here see the discussions in Refs. [54,55,56].)

Another interesting problem is to study the response of the fiber to an externally applied stress. Recent experiments have shown that the response of chromatin to an external mechanical stress can provide more insight into the DNA-histone interactions and the detailed conformation of the fiber [18,21,22,33,34]. This problem has been considered in several recent theoretical studies [17,18,36,38,54]. Finally, one may also consider an inhomogeneous fiber within the present model by assuming that the linker length may vary from one unit cell to the other. In this case, the fiber may exhibit overall deformations and large-scale conformational fluctuations [27].

A.N. is supported by the Royal Society, the Royal Academy of Engineering, and the British Academy.

References

1. A. U. Bielinska, J. F. Kukowska-Latallo, J. R. Baker Jr., *Biochim. Biophys. Acta* **1353**, 180 (1997).
2. P. L. Dubin, D.R. Rigsbee, L.-M. Gan and M. A. Fallon, *Macromolecules* **21**, 2555 (1988).
3. A. Tsuboi, T. Izumi, M. Hirata, J. Xia, P. L. Dubin and E. Kokufuta, *Langmuir* **12**, 6295 (1996).
4. F. Ganachaud, A. Elaissari, C. Pichot, A. Laayoun, and P. Cros, *Langmuir* **13**, 701 (1997).
5. J. K. Strauss and L. J. Maher, *Science* **266**, 1829 (1994).
6. J. Xia, P. L. Dubin and H. Dautzenberg, *Langmuir* **9**, 2015 (1993).
7. P. Haronska, T. A. Vilgis, R. Grottenmüller, and M. Schmidt, *Macromol. Theor. Simul.* **7**, 241 (1998).
8. D. I. Gittins and F. Caruso, *J. Phys. Chem. B* **105**, 6846 (2001).
9. D. I. Gittins and F. Caruso, *Adv. Mater.* **12**, 1947 (2000).
10. Y. Li, P. L. Dubin, H. A. Havel, S. L. Edwards and H. Dautzenberg, *Langmuir* **11**, 2486 (1995).
11. P. L. Dubin, M. E. Curran, and J. Hua, *Langmuir* **6**, 707 (1990).
12. D. W. McQuigg, J. I. Kaplan, and P. L. Dubin, *J. Phys. Chem.* **96**, 1973 (1992).
13. M. Jonsson and P. Linse, *J. Chem. Phys.* **115**, 3406 (2001).
14. M. Jonsson and P. Linse, *J. Chem. Phys.* **115**, 10975 (2001).
15. M. Skepö and P. Linse, *Macromolecules* **36**, 508 (2003).
16. B. Alberts, A. Johnson, J. Lewis, M. Raff, K. Roberts and P. Walter, *Molecular Biology of The Cell* (Garland Science (Taylor and Francis Group), New York, 2002).
17. H. Schiessel, W. M. Gelbart and R. Bruinsma, *Biophys. J.* **80**, 1940 (2001).
18. H. Schiessel, *J. Phys.: Condensed Matter* **15**, R699 (2003).
19. R. D. Kornberg and A. Klug, *Sci. Am.* **244**, 48 (1981).
20. K. Luger and T. J. Richmond, *Curr. Opin. Struct. Biol.* **8**, 33 (1998).
21. J. Widom, *J. Mol. Biol.* **190**, 411 (1986).
22. J. Yao, P. T. Lowary and J. Widom, *Proc. Natl. Acad. Sci.* **87**, 7603 (1990).
23. K. van Holde, *Nature* **362**, 111 (1993).
24. F. Thoma, Th. Koller and A. Klug, *J. Cell Biol.* **83**, 403 (1979).
25. J. Allan, T. Mitchell, N. Harborne, L. Boehm and C. Crane-Robinson, *J. Mol. Biol.* **187**, 591 (1986).
26. S. E. Gerchman, V. Ramakrishnan, *Proc. Natl. Acad. Sci. USA* **84**, 7802 (1987).
27. C. L. Woodcock, S. A. Grigoryev, R. A. Horowitz and N. Whitaker, *Proc. Natl. Acad. Sci.* **90**, 9021 (1993).
28. J. Bednar, R. A. Horowitz, S. A. Grigoryev, L. M. Caruthers, J. C. Hansen, A. J. Koster and C. L. Woodcock, *Proc. Natl. Acad. Sci.* **95**, 14173 (1998).
29. R. A. Horowitz, D. A. Agard, J. W. Sedat and C. L. Woodcock, *J. Cell Biol.* **125**, 1 (1994).
30. S. H. Leuba, G. Yang, C. Robert, B. Samori, K. van Holde, J. Zlatanova and C. Bustamante, *Proc. Natl. Acad. Sci. USA* **91**, 11621 (1994).
31. J. T. Finch and A. Klug, *Proc. Natl. Acad. Sci. USA* **73**, 1897 (1976).
32. A. Worcel, S. Strogatz, D. Riley, *Proc. Natl. Acad. Sci. USA* **78**, 1461 (1981).
33. Y. Cui and C. Bustamante, *Proc. Natl. Acad. Sci. USA* **97**, 127 (2000).
34. V. Katritch, C. Bustamante and W. K. Olson, *J. Mol. Biol.* **295**, 29 (2000).
35. G. Wedemann and J. Langowski, *Biophys. J.* **82**, 2847 (2002).
36. H. Schiessel, *Europhys. Lett.* **58**, 140 (2002).
37. J. Mozziconacci and J.-M. Victor, *J. Struct. Biol.* **143**, 72 (2003); J. Mozziconacci, C. Lavelle, M. Barbi, A. Lesne, J.-M. Victor, *FEBS Lett.* **580**, 368 (2006).
38. I. M. Kulić and H. Schiessel, *Phys. Rev. Lett.* **92**, 228101 (2004).
39. C. L. Woodcock, *Curr. Opin. Struct. Biol.* **16**, 213 (2006).
40. T. Schalch, S. Duda, D. F. Sargent, and T. J. Richmond, *Nature* **436**, 138 (2005).
41. B. Dorigo, T. Schalch, A. Kulangara, S. Duda, R.R. Schroeder, T. J. Richmond, *Science* **306**, 1571 (2004).
42. P. J. J. Robinson, L. Fairall, Van A. T. Huynh, and D. Rhodes, *Proc. Natl. Acad. Sci.* **103**, 6506 (2006).
43. A. T. Huynh, P. J. J. Robinson, and D. Rhodes, *J. Mol. Biol.* **345**, 957 (2005).

44. J. Langowski and D. W. Heermann, *Semin. Cell Dev. Biol.* **18**, 659 (2007); J. Langowski, *Eur. Phys. J. E* **19**, 241 (2006). F. Aumann, F. Lankas, M. Caudron and J. Langowski, *Phys. Rev. E* **73**, 041927 (2006).
45. P. M. Diesinger, D. W. Heermann, *Phys. Rev. E* **74**, 031904 (2006).
46. D. A. Beard, T. Schlick, *Structure*. **9**, 105 (2001); J. Sun, Q. Zhang and T. Schlick, *Proc. Natl . Acad. Sci . USA* **102**, 8180 (2005)
47. G. Arya, Q. Zhang, and T. Schlick, *Biophys. J.* **91**, 133 (2006).
48. K. van Holde and J. Zlatanova, *Semin. Cell Dev. Biol.* **18**, 651 (2007).
49. H. Wong, J.-M. Victor and J. Mozziconacci, *PLoS ONE* **2**, e877 (2007).
50. M. Depken and H. Schiessel, *Biophys. J.* **96**, 777 (2009).
51. M. Emanuel, N. H. Radja, A. Henriksson and H. Schiessel, *Phys. Biol.* **6**, 025008 (2009).
52. M. Kruithof, F.-T. Chien, A. Routh, C. Logie, D. Rhodes and J. van Noort, *Nat. Struct. Mol. Biol.* **16**, 534 (2009).
53. A. Routh, S. Sandin and D. Rhodes, *Proc. Natl Acad. Sci.* **105**, 8872 (2008).
54. K. K. Kunze and R. R. Netz, *Phys. Rev. Lett.* **85**, 4389 (2000); *Phys. Rev. E* **66**, 011918 (2002).
55. H. Boroudjerdi, R. R. Netz, *Europhys. Lett.* **64**, 413 (2003); **71**, 1022 (2005); *J. Phys.: Condens. Matter* **17**, S1137 (2005).
56. H. Boroudjerdi, *Charged Polymer-Macroion Complexes*, PhD thesis (Potsdam University, Potsdam, Germany, 2005).
57. H. Boroudjerdi, Y.-W. Kim, A. Naji, R.R. Netz, X. Schlagberger, A. Serr, *Phys. Rep.* **416**, 129 (2005).
58. Note that we set the linear charge density of DNA to the maximal value and treat it as constant. This turns out to be a good approximation for moderate to high salt concentration—see R.R. Netz and H. Orland, *Eur. Phys. J. E* **11**, 301 (2003).
59. M. Rief, H. Clausen-Schaumann and H. Gaub, *Nat. Struct. Biol.* **6**, 346 (1999).
60. C. Frontali, E. Dore, A. Ferrauto and E. Gratton, *Biopolymers* **18**, 1353 (1979).
61. W. H. Press, B. P. Flannery, S. A. Teukolsky and W. T. Vetterling, *Numerical Recipes in C* (Cambridge University Press, Cambridge, 1998)
62. S. Y. Park, R. F. Bruinsma, and W. M. Gelbart, *Europhys. Lett.* **46**, 454 (1999).
63. A. Yu. Grosberg, T. T. Nguyen, and B. I. Shklovskii, *Rev. Mod. Phys.* **74**, 329 (2002).
64. R. R. Netz and J.-F. Joanny, *Macromolecules* **32**, 9026 (1999).